1   **Residual Temperature Bias Effects in Stratospheric Species Distributions from LIMS**

3   Ellis Remsberg[1], V. Lynn Harvey[2], Arlin Krueger[3], and Murali Natarajan[1]

5   [1]Science Directorate, NASA Langley Research Center, 21 Langley Blvd, Mail Stop 401B,
6   Hampton, VA 23681, USA

7   [2]Laboratory for Atmospheric and Space Physics, University of Colorado Boulder, 3665
8   Discovery Drive, Boulder, CO 80303, Colorado, USA

9   [3]Emeritus Senior Scientist, Code 614 Atmospheric Chemistry and Dynamics Laboratory, NASA
10   Goddard Space Flight Center, Greenbelt, MD 20771, USA

14   Correspondence to: Ellis Remsberg (ellis.e.remsberg@nasa.gov)

17   (For submission to Atmospheric Measurement Techniques Journal)

18   January, 2021

20   **Abstract**

21   The Nimbus 7 Limb Infrared Monitor of the Stratosphere (LIMS) instrument operated from

22   October 25, 1978, through May 28, 1979. Its Version (V6) profiles were processed and archived

23   in 2002. We present several diagnostic examples of the quality of the V6 stratospheric species

24   distributions based on their Level 3 zonal Fourier coefficient products. In particular, we show

25   that there are small differences in the ascending (A) minus descending (D) orbital temperature-

26   pressure or T(p) profiles (their A-D values) that affect (A-D) species values. Systematic A-D

27   biases in T(p) can arise from small radiance biases and/or from viewing anomalies along orbits.

28   There can also be (A-D) differences in T(p) due to not resolving and correcting for all of the

29   atmospheric temperature gradient along LIMS tangent view-paths. An error in T(p) affects

30   species retrievals through: (1) the Planck blackbody function in forward calculations of limb

31   radiance that are part of the iterative retrieval algorithm of LIMS, and (2) the registration of the

32   measured LIMS species radiance profiles in pressure-altitude, mainly for the lower stratosphere.

33   There are clear A-D differences for ozone, H_2O, and HNO_3, but not for NO_2. Percentage

34   differences are larger in the lower stratosphere for ozone and H_2O because those species are

35   optically thick. We evaluate V6 ozone profile biases in the upper stratosphere with the aid of

36   comparisons against a monthly climatology of UV-ozone soundings from rocketsondes. We also

37   provide results of time series analyses of V6 ozone, H_2O, and potential vorticity for the middle

38   stratosphere to show that their average (A+D) V6 Level 3 products provide a clear picture of the

39   evolution of those tracers during northern hemisphere winter. We recommend that researchers

40   use the average V6 Level 3 product for their science studies of stratospheric ozone and H_2O, but

41   keeping in mind that there are uncorrected NLTE effects in daytime ozone in the lower

42   mesosphere and in daytime H_2O in the uppermost stratosphere. We also point out that the

43   present-day Sounding of the Atmosphere using Broadband Emission Radiometry (SABER)

44   experiment provides measurements and retrievals of temperature and ozone that are more nearly

45   free of anomalous diurnal variations and of effects from gradients at low and middle latitudes.

1 Introduction and objectives

The historic Nimbus 7 Limb Infrared Monitor of the Stratosphere (LIMS) experiment provided data on the middle atmosphere from October 25, 1978, through May 28, 1979, for scientific analysis and for comparisons with atmospheric models (Gille and Russell, 1984). Remsberg et al. (2007) describe characteristics of the ozone profiles of the LIMS Version 6 (V6) dataset. Notably, V6 corrects for a high ozone bias in the lowermost stratosphere of the previous Version 5 (V5) profiles, as shown by comparisons of the V6 profiles with ozonesonde data in Remsberg et al. (2007; 2013). Remsberg et al. (2009) report on improvements in the profiles and distributions of V6 water vapor (H_2O) within the lower stratosphere, where temperature and interfering radiances from the oxygen continuum are more accurate than in the processing of V5. Finally, Remsberg et al. (2010) contain information on the V6 improvements of nitric acid (HNO_3) and, in particular, nitrogen dioxide (NO_2).

Frith et al. (2020) reported on modeled estimates of diurnal ozone variations, as a function of latitude, altitude, and season. In general, their modeled results are in accord with observed ozone variations from both satellite ultraviolet (uv) and microwave measurements. However, the ozone distributions from the infrared measurements of LIMS show some anomalously large day/night differences in the middle stratosphere (Remsberg et al., 1984; 2007). LIMS ozone and H_2O are quite sensitive to small biases of the LIMS temperature versus pressure, or T(p), due to nonlinear effects of the Planck blackbody function in forward radiance calculations that are part of the LIMS retrieval algorithm (Gille et al., 1984; Remsberg et al., 2004). Consequently, temperature bias is the largest source of ozone and H_2O error, by far, although small bias effects from T(p) are hard to verify from correlative comparisons of individual profiles. The LIMS orbital line-of-site to its tangent layer is nearly in a meridional direction or along horizontal temperature gradients (Remsberg et al., 1990). Roewe et al. (1982) consider line-of-sight radiance gradient corrections for the LIMS species retrievals, while Gille et al. (1984) employ corrections based on the T(p) gradient. We will show that while the LIMS algorithm makes first-order corrections for T(p) gradients, residual bias effects are still apparent in the V6 species distributions.

76   This study considers the distributions of V6 T(p) plus plots of ascending (A) minus descending

77   (D) orbital differences (A-D) for both temperature and species, as diagnostics for the effects of

78   residual bias errors in T(p). We evaluate those effects using plots of the LIMS Level 3 (mapped)

79   products (Remsberg et al., 1990; Remsberg and Lingenfelser, 2010) and their monthly zonal

80   mean distributions that are part of the SPARC Data Initiative (SPARC, 2017). Section 2 gives a

81   brief review of the characteristics and retrieval algorithms for V6 temperature and species.

82   Section 3 reviews the measurement, retrieval, and day/night differences for temperature. Section

83   4 relates small temperature biases to the anomalous A-D values in the LIMS monthly species

84   distributions for March 1979. Section 5 compares V6 daytime ozone with rocketsonde UV-filter

85   ozone (ROCOZ) profile data for the upper stratosphere and lower mesosphere. We interpret the

86   comparisons according to their respective error estimates and by examining the profiles in the

87   context of hemispheric maps of the surrounding temperature and ozone fields from the Level 3

88   products. Section 6 contains results of time series of northern hemisphere (NH) distributions of

89   V6 ozone and H_2O on the 850 K potential temperature surface (~10 hPa), as indications of the

90   quality of averages of their V6 data. Section 7 summarizes our findings about the V6 species

91   and our recommendations for scientific studies of them. We also point out why the follow-on

92   experiment, Sounding of the Atmosphere using Broadband Emission Radiometry (SABER),

93   provides measurements and retrievals of temperature that are nearly free of anomalous A-D

94   differences at low and middle latitudes.

95

96   **2   Characteristics of the V6 Level 3 ozone, temperature, and water vapor**

97   *2.1 Daily mapped data*

98   The V6 algorithm accounts for low-frequency spacecraft motions that affect how the LIMS

99   instrument views the horizon and the subsequent registration of its measured radiance profiles in

100 pressure-altitude (Remsberg et al., 2004). Retrieved ozone, temperature, and geopotential height

101 (GPH) profiles extend from 316 hPa to ~0.01 hPa and have a point spacing of ~0.88 km with a

102 vertical resolution of ~3.7 km. H_2O, HNO_3, and NO_2 data are limited to the stratosphere (~100

103 hPa to 1 hPa). Processing of the original V5 T(p) profiles occurred at a rather coarse vertical

104 point spacing of ~1.5 km and for every ~4 degrees of latitude. Retrievals for V6 occur at every

105 ~1.6 degrees of latitude along orbits and resolve the horizontal temperature structure better.

106   However, the line-of-sight T(p) gradients for both the V5 and V6 processing algorithms are from

107   daily maps of the combined V5 (A+D) temperature fields on pressure surfaces.

108

109   Mapping of the V6 profiles to a Level 3 product occurs at 28 vertical levels, as opposed to just

110   18 levels for V5. The sequential-estimation mapping algorithm for V6 (Remsberg and

111   Lingenfelser, 2010) employs a shorter relaxation time of about 2.5 days for its zonal wave

112   coefficients, compared with ~5 days for V5. The mapping algorithm is insensitive to the very

113   few large, unscreened ozone mixing ratio values within the lower stratosphere, as noted in

114   Remsberg et al. (2013, Fig. 1a). LIMS made measurements with a duty cycle of up to 11 days

115   on and 1 day off, and the mapping algorithm interpolates the profile data in time to provide a

116   continuous, 216-day set of daily zonal coefficients. Daily maps also provide a spatial context for

117   the individual V6 profiles and are helpful for interpreting comparisons with auxiliary data sets,

118   especially during dynamically disturbed periods.

119

120   *2.2 Monthly zonal average V6 ozone, temperature, and water vapor*

121   We generated monthly zonal mean distributions from the daily Level 3 files of temperature and

122   species and supplied them to the SPARC Data Initiative or SPARC-DI (SPARC, 2017).

123   Although the V6 ozone for SPARC-DI extends up to only the 0.1-hPa level (~64 km), Figure 1

124   updates the combined (A+D), monthly ozone for March 1979 to its highest level of about 0.015

125   hPa (~75 km). Retrieved daytime ozone contributes to the (A+D) ozone in Fig. 1 and has a large

126   positive bias throughout the mesosphere because the LIMS algorithms do not account for non-

127   local thermodynamic equilibrium (NLTE) effects from either ozone (Solomon et al., 1986;

128   Mlynczak and Drayson, 1990) or CO_2 (Edwards et al., 1996; Manuilova et al., 1998). However,

129   the V6 nighttime ozone is essentially free of those NLTE effects below about the 0.05-hPa level.

130   We also screened the SPARC-DI product of daily zonal mean ozone values (<0.1 ppmv) near the

131   tropical tropopause, as recommended in Remsberg et al. (2013). This study focuses on the

132   quality of V6 ozone in the stratosphere.

133

134   Figure 1 shows that ozone has largest mixing ratios at about 10 hPa near the Equator (~10.8

135   ppmv), decreasing sharply above and below that level. Maximum mixing ratios at the middle to

136   high latitudes occur closer to 3 hPa, due to larger zenith angles and longer paths of the uv light

137   for the production of its atmospheric ozone. Remsberg et al. (2007) compared V6 ozone and

138   Solar Backscatter UltraViolet (SBUV) Version 8.0 ozone and reported that V6 ozone is larger

139   (by 4 to 12%) in the upper stratosphere, although the differences are within the combined errors

140   of V6 and SBUV. However, the monthly comparisons at 4 hPa indicate that those differences

141   increase from November to May. Sun and Leovy (1990, their Fig. 1) also compared Equatorial

142   ozone time series from LIMS and SBUV, and they found that their monthly differences for the

143   upper stratosphere changed with the descent of the semi-annual oscillation (SAO). Most likely,

144   LIMS and SBUV do not resolve the vertical response of ozone to the SAO equally well.

145

146   Figure 2 shows the March zonal mean V6 T(p) distribution from SPARC-DI. Monthly T(p)

147   extends to near the 0.01-hPa level and has values every 5° of latitude. T(p) has a maximum

148   value of about 275 K at the stratopause and minimum values approaching 195 K near the

149   mesopause and at the tropical tropopause. Radiances from the two 15-μm CO_2 channels for

150   retrievals of T(p) are free of NLTE effects below about the 0.05-hPa level (~70 km) (Lopez-

151   Puertas and Taylor, 2001). Estimates of a bias in V6 T(p) are in Table 1 (row 2), according to

152   Remsberg et al. (2004, their Table 2, row g) but not including any error due to temperature

153   gradients. Estimates of bias errors for ozone due to those T(p) errors are in Table 1 (row 3); a

154   positive bias in temperature leads to a negative bias in retrieved ozone (and the other species) via

155   the effect of the Planck function on radiance calculations. In principle, one may also infer the

156   quality of the V6 temperatures based on independent estimates of the quality of the retrieved

157   ozone. Table 1 (last row) compares V6 T(p) for March 1979 at 38°N with that from the

158   temperature climatology at 40°N from Barnett and Corney (or BC, 1985). Those (V6 – BC)

159   temperature values include a five-point running average of the SPARC-DI V6 monthly T(p)

160   profile above the 30-hPa level to account for the broader vertical weighting functions of the

161   satellite measurements of BC. The difference profiles, V6-BC, have values of the order of the

162   bias estimates for V6 T(p) (in row 2). The larger difference of -4.4 K at 3 hPa indicates the

163   redistribution of northern hemisphere temperature following the final stratospheric warming and

164   split vortex that is specific to late February 1979.

165

166   Figure 3 shows V6 zonal average H_2O for March 1979 from SPARC-DI. Highest values of H_2O

167   are at upper altitudes (> 6.0 ppmv) and are due to the oxidation of methane (CH_4) to H_2O,

168   followed by its net transport and accumulation at higher latitudes. H_2O is effectively a tracer of

169   the mean meridional circulation, which moves upward from the tropical tropopause to the middle

170   stratosphere and then poleward toward higher latitudes. Minimum zonal-mean values of H_2O are

171   of order 3.5 ppmv in the tropics between 50 and 70 hPa. The sharply increasing H_2O near the

172   tropical tropopause may be due, in part, to residual radiance from cirrus cloud tops. The V6

173   species have a first order screening for clouds at latitudes between ±30° and for pressure-

174   altitudes below 45 hPa, according to a threshold criterion of the vertical slope of the co-located

175   ozone mixing ratio profiles (see Sections 2.2 in Remsberg et al., 2007; 2009). Locations of cloud

176   tops are in separate daily files that are a part of the V6 Level 2 or daily profile data set. NLTE

177   processes also cause enhancements of H_2O radiance near the stratopause during daytime. Those

178   uncorrected NLTE effects extend downward to lower altitudes for retrieved V6 H_2O, although

179   the effects are small for the middle and lower stratosphere (Mertens et al., 2002). Estimates of

180   the effect of temperature bias for V6 H_2O are in Table 1 (row 4) from Remsberg et al. (2009).

181

182   **3   Measurement, retrieval, and day/night differences for temperature**

183   Nimbus 7 was in a near-polar orbit, and LIMS made measurements at ~1 pm local time along its

184   ascending (A or south-to-north traveling) orbital segments and at ~11 pm for its descending (D

185   or north-to-south traveling) segments. The A-D time difference is of the order of 10 hours

186   because LIMS viewed the atmosphere 146.5° clockwise of the spacecraft velocity vector or 33.5°

187   counterclockwise from its negative velocity vector, as seen from overhead. In other words,

188   LIMS viewed atmospheric tangent layers in opposing meridional directions for the NH and

189   through the tropics or toward the SSE along A segments and toward the NNW along D segments

190   (Gille et al.,, 1984; Remsberg et al., 1990). The A and D view paths for middle latitudes of the

191 SH are more nearly in a zonal direction and toward the NNW, respectively, due to the orbital

192 inclination of Nimbus 7.

193

194 Figure 4 shows V6 A-D temperatures for March. The differences of the upper stratosphere

195 indicate how well the effects of the temperature tides have been resolved (Remsberg et al.,

196 2004). Tropical differences are due mainly to diurnal tides, and they become large in the

197 mesosphere. Tidal amplitudes for the tropics increase with altitude in Fig. 4, ranging from -2 K

198 at 15 hPa to +4 K at 1.5 hPa. Those V6 tidal variations agree qualitatively with ones from rocket

199 Datasonde profiles (Hitchman and Leovy, 1985; Finger et al., 1975). Fig. 4 also shows the

200 expected 180° change of tidal phase for A-D T(p) from the tropics to subtropics. Accurate

201 determinations of T(p) versus latitude depend critically on knowledge of the Nimbus 7 spacecraft

202 attitude. That information for a complete orbit comes empirically from profiles of calculated-to-

203 measured radiance ratios for the LIMS narrow CO_2 channel and can lead to a bias error for A-D

204 T(p). Although orbital attitude bias will affect T(p) at all altitudes, that error source is small

205 according to the good comparisons of the LIMS-derived geopotential heights versus those from

206 operational analyses at both the 10-hPa and 46-hPa levels (Remsberg et al., 2004). Even so, Fig.

207 4 also shows that there are residual A-D T(p) differences at 70 hPa that are opposite in sign at

208 40°S and 30°N, or just where there are large, opposing meridional gradients in T(p) in Fig. 2.

209

210 Measured ozone radiance profiles contain the full effects of any atmospheric variations in T(p).

211 As an example, Figure 5 shows zonal mean, ozone radiance differences (A-D) for one day

212 (March 15). Radiance differences in the tropics have a change in sign from positive at 3 hPa to

213 negative in the lower mesosphere, and they correspond directly with the A-D changes of

214 temperature in Fig. 4. Positive A-D radiances at middle latitudes of the lower mesosphere are

215 due to the dominance of NLTE daytime radiances from CO_2 and O_3, as compared with the tidal

216 effects from T(p).

217

218 There are negative A-D ozone radiances of up to -5% at the northern middle latitudes of the

219 stratosphere, and they are a result of the meridional decrease of T(p) (in Fig. 2) from the northern

220   subtropics toward higher latitudes. More of the measured radiance in that region comes from the

221   front end of the tangent layer or from the colder side on the A orbital segment and from the

222   warmer side on the D segment, leading to negative A-D radiances. Gille et al. (1984) found that

223   the corresponding A-D temperature differences extend to 4 K or even greater at high northern

224   latitudes. The LIMS algorithms for temperature and species account for horizontal temperature

225   gradients on a pressure surface, in the following manner. Daily, near-global temperature fields

226   were obtained from a mapping of the T(p) profiles from a V5 first-pass retrieval. The mapped

227   fields are at 18 separate pressure levels (spaced vertically by 2.3 to 4.3 km, depending on level).

228   Temperature gradients for each profile were determined from the maps, according to the LIMS

229   tangent-path viewing direction in longitude and latitude, and new, second-pass T(p) retrievals

230   were performed taking account of those gradients. V5 gradient estimates from the similar V5

231   Level 3 map product were used for the processing of the V6 profiles. The T(p) gradient values

232   for each profile are on the archived V6 Level 2 files and used for retrievals of the species. While

233   both the V5 and V6 temperature profile biases become smaller after gradient correction, one

234   must remember that our analyzed temperature gradient information is approximate.

235

236   The A-D T(p) differences may still be of order 1 to 2 K after correction (see Figs. 4 and 5 in

237   Gille et al., 1984; Remsberg et al., 2004 and 2007). Kiefer et al. (2010) analyzed for the effects

238   of a T(p) gradient in more detail using data from the limb-infrared, Michelson Interferometer for

239   Passive Atmospheric Sounding (MIPAS) experiment. They confirm the need to correct for T(p)

240   gradients in the respective A and D views for accurate retrievals of species from the MIPAS A

241   and D radiance profiles. We emphasize that the T(p) gradients for LIMS V6 are from daily

242   surface maps of average (A+D) V5 temperature fields, where the meridional resolution of the V5

243   fields is no better than half that of V6, or 4° versus 2° of latitude. Those V5 average (A+D) T(p)

244   gradients underestimate the true atmospheric gradients and can result in slight biases between the

245   A and D T(p) values for V6 at a given latitude.

246

247   V6 retrievals of T(p) employ a starting reference pressure level P_o near 20 hPa (~26 km relative

248   altitude) plus hydrostatic conversions to pressure-altitude that extend both upward and

249   downward from P_o. The algorithm makes forward radiance calculations for the two broadband

250   CO_2 channels and compares them with their measured radiance profiles. T(p) (A-D) differences

251   of the same sign will impart growing A-D radiance versus pressure differences away from P_o.

252   Both P_o and T(p) undergo iteration until the calculated and measured, tangent layer radiances

253   agree to within the noise levels of the measured radiances over the pressure range of 2 to 20 hPa.

254   Yet, the noise value is nearly 2% of the signal at 2 hPa for the narrow CO_2 channel. This

255   pressure level is where the diurnal temperature tide has a larger amplitude and can impart a

256   systematic, A-D bias in P_o. A-D bias errors in radiance versus pressure are also significant; a

257   radiance calibration error of 1% causes a 0.6 K error in T(p) for the middle and upper

258   stratosphere (Remsberg et al., 2004, Table 3). Another possible source of (A-D) bias for T(p)

259   can arise from a residual uncertainty of the viewing attitude of LIMS along an orbit, its empirical

260   "twist factor".

261

262   Roewe et al. (1982) showed that adjustments for horizontal gradients in T(p) affect species

263   retrievals through calculations of the Planck blackbody radiance, as well as from the registration

264   of their radiance versus pressure profiles, mainly in the lower stratosphere. The region of

265   negative, A-D ozone channel radiance in Fig. 5 has values that increase toward the lower

266   stratosphere because of persistent A-D T(p) biases plus the hydrostatic registration of the

267   measured radiance profiles with pressure-altitude. The radiance differences are negative at

268   middle latitudes of the NH but positive in the SH. Ozone radiance at 10 hPa (not shown)

269   increases from 40°N to 18°N, holds nearly steady in the tropics, and decreases from 20°S to

270   40°S, mainly due to the changing ozone with latitude (Fig. 1). Gordley and Russell (1981)

271   showed that the bulk of the LIMS broadband ozone radiance for the middle and lower

272   stratosphere comes from the near side of the tangent layer (displaced toward the satellite by

273   about 300 to 500 km or ~3° to 6° of latitude). That tangent layer weighting explains part of the

274   observed change of sign of the A-D radiances between the two hemispheres in Fig. 5.

275   Nevertheless, the mass path algorithm of the V6 forward model simulates radiance along a well-

276   resolved limb path, using rigorous ray tracing methods, including refraction effects and the first-

277   order corrections for temperature gradients, and assigns an observed tangent altitude

278   corresponding to the center of the measurement field-of-view.

279

280 Roewe et al. (1982) also showed that adjustments for the path gradients of the ozone mixing ratio

281 itself imparts only small A-D mixing ratio differences (~2%). Thus, V6 retrievals do not account

282 for species gradients. The V6 algorithms are no longer operational for further detailed studies of

283 the effects of T(p) gradients for the LIMS species. Instead, in the next section we present

284 diagnostic plots based on the V6 Level 3 data themselves to indicate that there are residual biases

285 in the distributions of V6 T(p) and that they carry over to the V6 species.

286

287 **4   Day/night differences in V6 species**

288 *4.1 Upper stratospheric ozone and H_2O*

289 Remsberg et al. (1984; 2007) reported on the occurrence of day/night, or the A-D ozone values;

290 those results are similar for V5 and V6. Figure 6 shows the distribution of V6 A-D ozone for

291 March as divided by the zonal mean ozone, such that the pattern of systematic differences is a

292 percentage of the zonal average ozone. Photochemical calculations by Haigh and Pyle (1982)

293 predict about a -2% change in ozone for a +1 K change in T(p) at 1.5 hPa. The V6 tropical

294 ozone differences in Fig. 6 grow to nearly -3% near 1 hPa and are opposite in sign to the

295 temperature tides of Fig. 4. Thus, the V6 ozone of the tropical upper stratosphere agrees

296 reasonably with effects from the observed temperature tides.

297

298 Sakazaki et al. (2013, their Fig. 4) also reported diurnal model calculations of tropical day-night

299 ozone values of -3.5% at 44 km (~1.7 hPa) at the local times of the LIMS observations; their

300 microwave observations of ozone agree with them. They also obtained A-D ozone variations of

301 +3.5% at 34 km (~6 hPa) from the photochemistry of odd oxygen during daytime, and those

302 differences decay away from the Equator. Yet, the V6 A-D tropical ozone differences of Fig. 6

303 are nearly twice as large at 6 hPa, and they disagree with modeled changes in Frith et al. (2020).

304 There are also separate, rather large V6 ozone differences at middle latitudes of the upper

305 stratosphere, where effects from temperature tides are small. The rather large A-D ozone values

306 (~4 to 6%) at SH middle latitudes correspond to where the A-D ozone radiances in Fig. 5 are

307 increasing with altitude by +2 to +4% and where A-D T(p) is weakly negative. While these

308 results are consistent with the effects of temperature on retrieved ozone through the V6

309   algorithm, the ozone radiances may also have an A-D pressure registration bias due to the

310   persistently, negative A-D T(p) in that region. The axis of the positive A-D ozone anomaly at

311   NH middle latitudes in Fig. 6 overlays the region of rather large, meridional T(p) gradients in

312   Fig. 2.

313

314   Figures 7 and 8 provide supporting evidence that uncorrected, residual temperature gradients are

315   a likely cause of the A-D ozone anomalies in Fig. 6. Fig. 7 shows zonal (wave) standard

316   deviations (SD) about the zonal average of the combined (A+D) temperature fields for March,

317   where the SD values are from the LIMS SPARC-DI data product. There is significant zonal

318   wave activity at middle to high latitudes in both the NH and SH, and one must account for their

319   separate A and D horizontal gradients for accurate ozone retrievals. Fig. 8 is the corresponding,

320   zonal wave standard deviations for ozone that have a maximum value of 0.40 ppmv near 65°N

321   and 1 hPa, or where transport affects the ozone as well as chemistry.

322

323   V6 H_2O retrievals are more sensitive than ozone to biases in T(p) at 3 hPa (in Table 1) because

324   most of the V6 H_2O radiance comes from its strong, nearly saturated lines. Figure 9 shows H_2O

325   A-D mixing ratio values for March. Both species are altered by horizontal gradients in T(p) in

326   the same way in calculations of their Planck radiances. The locus of maximum percentage

327   difference for H_2O in the SH middle to upper stratosphere differs from that for ozone (Fig. 6)

328   because their respective mixing ratios also have gradients that differ. The effect of the tropical

329   temperature tide on H_2O is not apparent at 1.5 hPa because of the excess of NLTE radiance for

330   V6 daytime H_2O at and above that level.

331

332   *4.2 Middle and lower stratosphere ozone and H_2O*

333   V6 A-D ozone mixing ratio in Fig. 6 is near zero at 20 hPa. This feature occurs where V6 A-D

334   for T(p) in Fig. 4 is also small, or where there is iteration of P_o and a hydrostatic integration both

335   above and below that level. The ozone differences become negative below that level across the

336   tropics and in the NH, where the vertical gradient of ozone (Fig. 2) is large and subject to small

337   A-D differences for the registration of the ozone radiance profiles. However, the ozone

338   differences at SH middle latitudes remain positive down to the 100-hPa level; only tangent views

339   along the descending orbital path are in a nearly meridional direction at those latitudes. In

340   particular, the A-D ozone values in Fig. 6 are rather large at 40°S and at 30°N (40 to 100 hPa),

341   and they are opposite in sign to the A-D T(p) differences of order ±1 K in Fig. 4. This finding

342   agrees with the estimates of T(p) effects at 50 hPa in Table 1, where a bias of -1.3 K leads to a

343   +20% bias in ozone. The A-D temperature biases are large just where the meridional

344   temperature gradients are also large (Fig. 2) and where corrections for them may be too small.

345

346   A-D values for H_2O in Fig. 9 have an opposite character from those of ozone from 50 to 100 hPa

347   because the vertical gradient of H_2O in Fig. 3 is also opposite that of ozone in the lowermost

348   stratosphere. This finding is a clear indication of how the same A-D T(p) biases can affect

349   retrieved ozone and H_2O differently. The few correlative balloon measurements of H_2O during

350   1978/1979 are too uncertain to judge whether the V6 H_2O A or D profiles are more accurate.

351

352   One particular feature is that both A-D ozone and H_2O are positive and approach 8% at about 10

353   hPa and 25°N. The SD values for temperature and ozone show local increases there, too. Fig.

354   10 gives details of the NH distribution of V6 ozone on the 10-hPa surface for one day, March 15,

355   from a gridding (at 2° lat; 5.625° long) of its 13 zonal Fourier coefficients (a zonal mean and 6

356   cosine and sine values) in the Level 3 product (Remsberg and Lingenfelser, 2010). There is a

357   meridional ozone gradient at the equatorward edge (~25°N) of a much larger mid latitude region

358   of near zero gradient—a result of effects of an efficient mixing with air from higher latitudes

359   during late winter. Zonal average, A-D temperatures at 10 hPa in Fig. 4 are of order -1 K at

360   15°N but then change to weakly positive at 25°N. The corresponding NH field of T(p) on March

361   15 is in Fig. 11, and it shows a narrow belt of slightly higher temperature near 25°N, or just

362   where the A-D meridional T(p) gradient has a change sign in Fig. 4. Such small T(p) differences

363   also affect the registration of the ozone and H_2O radiance profiles. There are unexpected,

364   tropical A-D ozone mixing ratios of order 5% at 10 hPa for all the LIMS months. Those

365   anomalies appear to migrate seasonally across the tropics and subtropics (see temperature and

366   ozone results for other selected months in the *Supplemental Material*).

367

368   *4.3 Stratospheric HNO₃ and NO₂*

369   LIMS HNO_3 is optically thin and its retrievals are much less sensitive to temperature bias via the

370   Blackbody function (Table 1, row 5). Its radiance profile measurements also come more nearly

371   from the center of the tangent layer, unlike those of ozone and water vapor. Maximum mixing

372   ratios for HNO_3 occur at about 20 hPa in the tropics and 30 hPa at high latitudes (e.g., as in Fig. 1

373   of Remsberg et al., 2010) or similar to those of ozone. Figure 12 is a plot of A-D for V6 HNO_3

374   (in %) for March for comparison with that of ozone in Fig. 6, and there are two important

375   differences between them. First, A-D for HNO_3 in the middle and upper stratosphere is

376   uniformly negative due to its photolysis during daytime, whereas A-D for ozone is slightly

377   positive from enhanced production during the day. Secondly, there are no apparent variations in

378   A-D for HNO_3 in the upper stratosphere at 40°S and near 10 hPa at 25°N from the effects of co-

379   located, horizontal temperature gradients. Yet, the patterns with latitude of A-D in the lower

380   stratosphere are very similar for both HNO_3 and ozone and indicate the effects of A-D

381   temperatures on the registration of the radiance profiles, prior to their retrieval to mixing ratios.

382

383   LIMS measured NO_2 radiances at around 1300 and 2300 hours from the Equator to 60°N but

384   changed quickly to 1445 and 2118 hours by 80°N. There is a more gradual change in viewing

385   times for the southern hemisphere from 1323 to 2237 hours at 20°S and then from 1545 and

386   2015 hours at 60°S, all due to the orbital viewing geometry of LIMS. V6 NO_2 mixing ratios

387   decrease rapidly after sunrise and then increase sharply again at sunset. There is also a slow

388   conversion of NO_2 to NO_3 and N_2O_5 after sunset, mainly in the middle stratosphere (Brasseur

389   and Solomon, 2005). Figure 13 shows a slightly different, but more standard diagnostic of NO_2

390   A to D ratios for March, and they vary according to the local times of the measurements.

391   However, note that the LIMS observations occurred beyond the day/night terminator at the

392   highest latitudes. V6 NO_2 has low S/N below about the 30-hPa level and is not accurate there;

393   elsewhere the A to D ratios should be representative.

394

395   V6 NO_2 is also sensitive to temperature bias (Table 1, row 6, and Remsberg et al., 2010). Fig. 13

396   shows a slight asymmetry of the 0.7 contour about the equator; that ratio are smaller in the

397   northern subtropics or opposite in magnitude to that expected from the effects of the T(p) bias in

398   Fig. 4. There is significant interfering radiance from H_2O in the NO_2 channel from the middle to

399   lower stratosphere (Russell et al., 1984), and recall that H_2O has its own T(p) bias effects (see

400   Fig. 9). Radiance from H_2O is also a larger correction for day versus night V6 NO_2. Thus,

401   although we expected to find temperature bias effects in V6 NO_2, indications of them are

402   somewhat ambiguous in Fig. 13.

403

404   **5 Ozone comparisons with rocket-borne measurements**

405   This section considers the quality of the V6 ascending (daytime) ozone of the middle and upper

406   stratosphere at NH middle latitudes; there is only one corresponding comparison for the

407   descending (nighttime) ozone (not shown, but see Remsberg et al., 1984, their Fig. 13). Krueger

408   (1973) developed meteorological rocket-borne, UV-absorption ozonesonde (ROCOZ)

409   instruments in the 1960s and 1970s and made routine soundings of middle atmosphere ozone.

410   To measure absorption of sunlight in three altitude regions between 15 and 60 km, ROCOZ used

411   four interference filters procured commercially in batches for uniformity. There were launches

412   of ROCOZ instruments for the validation of LIMS (seven flights) and of SBUV ozone at low-

413   (Natal, Brazil), mid- (Wallops Island, VA) and high- (Fort Churchill and Primrose Lake,

414   Canada) latitudes. Remsberg et al. (1984) reported on comparisons of the V5 ozone with

415   ROCOZ soundings and found mean differences (V5 minus ROCOZ) that varied from 5% in the

416   upper stratosphere to 16% in the lower stratosphere. The RMS differences were rather large

417   though (12% to 23%, respectively), and there were concerns about the stability of the batch of

418   UV interference filters used in the ROCOZ instruments from late 1978 through mid-1979.

419

420   An early 'ozone climatology' was produced from the greater than 200 ROCOZ soundings

421   launched between 1965 and 1990 at rocket ranges from the equator to high latitudes of both

422   hemispheres (Krueger, 1984; WOUDC). The ROCOZ flights include a SH latitude survey,

423   calibration flights for the Orbital Geophysical Observatory (OGO-4) UV spectrometer (London

424 et al., 1977), low latitude baseline flights from Antigua, high latitude flights from Fort Churchill

425 and Primrose Lake, validation flights for the Backscatter Ultraviolet (BUV) experiment on

426 Nimbus 4, and a regular monthly series of measurements from Wallops Island, VA. In fact, the

427 1976 U.S. Standard Atmosphere mid-latitude ozone model makes use of rocket data from seven

428 international experimenters, including ROCOZ (Krueger and Minzner, 1976).

429

430 Krueger (1984) also compiled separate monthly averages of soundings from Wallops Island

431 (38°N) during the period of March 1976 through September 1978. Uncertainty about the UV

432 filters was not at issue for those soundings. As an example, Fig. 14 compares the April average

433 from ROCOZ with the monthly zonal mean V6 Level 3 daytime ozone at 38°N for April 1979,

434 when wave activity and zonal variations about the V6 daily zonal means are <3%. Even though

435 the V6 profiles contain 18 values per decade of pressure (spaced ~0.88 km), we plot only every

436 other point because the V6 data carry an effective vertical resolution of ~3.7 km. The horizontal

437 bars at 0.3, 1, 2, and 10 hPa represent estimates of bias error for V6 ozone from Remsberg et al.

438 (2007, their Table 1). The ROCOZ profiles are averages of the three April soundings for 1976-

439 1978, and the horizontal bars at 0.5, 1.5, 3, 7, and 15 hPa are their estimated uncertainty of <10%

440 (or <7% for ozone number density versus altitude, plus <3% for the conversion to mixing ratio

441 versus pressure, as taken from Table II-7 of Krueger (1984)). Fig. 14 indicates agreement to

442 within the estimates of bias error for V6 ozone at most altitudes of the stratosphere. V6 ozone is

443 higher than ROCOZ ozone from ~2.0 to 0.3 hPa.

444

445 Figure 15 shows V6 daytime minus ROCOZ average profiles at Wallops Island (38°N) for

446 November, March, April, and May. The ozone differences are within their combined error

447 estimates for the middle stratosphere but are larger in the upper stratosphere and, especially, the

448 mesosphere. The increasingly positive, V6 day minus ROCOZ differences in the lower

449 mesosphere from winter to late spring are due to uncorrected NLTE effects for V6 from CO_2 and

450 ozone that increase toward lower solar zenith angles (Solomon et al., 1986; Mlynczak and

451 Drayson, 1990). On the other hand, the V6 daytime ozone of April and May is also larger than

452 ROCOZ ozone at 1.5 to 3 hPa, where NLTE should not be an issue (Edwards et al., 1996).

453 While there may be excess V6 ozone due to a slight negative bias for V6 T(p) at those pressure-

454   altitudes, it may also be that the ROCOZ climatology at Wallops Islands is not truly

455   representative of zonal average ozone for those months of 1979. In the next section, we report

456   on time series of fields of potential vorticity, ozone, and H_2O from their V6 Level 3 combined

457   (A+D) products for the middle stratosphere, where those parameters are not expected to have

458   diurnal variations and should serve as tracers of atmospheric transport.

459

460   **6 Seasonal transport of V6 ozone and water vapor**

461   Dunkerton and DeLisi (1986) made use of LIMS V5 GPH and temperature data to calculate

462   potential vorticity (PV) and then to show how PV evolved in the NH on the 850 K potential

463   temperature (~10 hPa) surface during January and February 1979. Butchart and Remsberg (BR,

464   1986) also calculated PV from the V5 data and plotted its evolution during the winter of 1978-

465   1979 in terms of the fractional area of the NH enclosed by the horizontal projection of a given

466   PV contour on the 850 K surface. These so-called, area diagnostic analyses of BR work well for

467   a parameter like PV that is monotonic with latitude, having its highest value at the Pole.

468

469   New time series analyses of PV from the combined V6 data are in Fig. 16, calculated from the

470   Level 3, daily 6-wavenumber, zonal coefficients of GPH and temperature. Equivalent latitude

471   (on the right ordinate) represents the latitude at which a zonally symmetric PV contour would lie

472   if it enclosed the given fractional area shown on the left ordinate. PV data for Fig. 16 have a 7-

473   day smoothing, and the NH fractional area extends only to 20° equivalent latitude because

474   calculations of absolute vorticity are not so accurate near the Equator. The PV results for V6 are

475   nearly identical to those for V5 in BR (their Fig. 4). Notably, the polar vortex (defined by

476   highest PV values) erodes during winter and the adjacent 'surf-zone', having much lower PV

477   gradients, expands in area due to the 'breaking' of planetary waves and the associated meridional

478   mixing of vortex and lower latitude air.

479

480   Ozone is an effective tracer of the transport of air in and around the winter polar vortex on the

481   850 K surface (~10 hPa) (Leovy et al., 1985). Ozone also varies nearly monotonically at this

482   level, but with highest values at low latitudes and lowest values near the Pole. BR analyzed the

483   evolution of V5 ozone (see their Fig. 10b). They compared its changes with those of PV and

484   found good correspondence for the large-scale features of the two distributions. Fig. 17 is the

485   new ozone time series at 850 K from the gridded V6 data, and it compares well with the

486   calculations of BR from the V5 ozone. One significant change with V6 is that the ozone

487   contours of 6.8 through 7.2 ppmv of early February indicate very weak gradients within the surf

488   zone, as it expands following the major warming event of late January. There is also an

489   associated, diabatic cross-isentropic transport of ozone within the surf zone during that time

490   (e.g., Butchart, 1987). The improved continuity of the ozone time series from V6 is a result of

491   the better spatial sampling for the radiances, of the retrievals of T(p) profiles, and of the

492   corresponding changes for the registration of the ozone radiance profiles and retrieved ozone

493   mixing ratios.

494

495   Water vapor is also a tracer of the net transport in the middle stratosphere. Figure 18 shows the

496   corresponding time series of V6 H_2O at 850 K. V6 H_2O mixing ratio contours vary more

497   smoothly than those from the V5 data in BR (their Fig. 12); the retrieved V6 H_2O profiles are

498   better resolved spatially and have better precision. There is good correspondence between H_2O,

499   PV, and ozone for the location and evolution of the edge of the polar winter vortex and for the

500   expansion of the region of weak gradients at middle latitudes. Low values of H_2O extend to the

501   northern middle latitudes and high values of H_2O descend within the polar vortex from

502   November through January, indicating an acceleration of the Brewer/Dobson circulation during

503   that winter. There is also a modest expansion of weak H_2O gradients between 40°N to 60°N

504   equivalent latitude from mid-November to mid-December. This region coincides with the time

505   of the Canadian warming and an exchange of air between polar and middle latitudes.

506

507   **7 Summary and recommendations**

508   This study provides some insight about the quality of the LIMS V6 Level 3 product and about

509   the generation of daily gridded species distributions on pressure surfaces. Monthly zonal mean

510   distributions are available within the SPARC-DI database for comparisons with model

511   simulations of middle atmosphere species. We also provide the corresponding monthly zonal

512   mean distributions of temperature for SPARC-DI and diagnostic evidence of effects of residual

513   temperature biases in the V6 ozone, H_2O, and HNO_3 distributions. Those species exhibit

514   ascending minus descending (A-D or day minus night at most latitudes) anomalies, especially in

515   the middle and lower stratosphere. In particular, the A-D ozone and H_2O values are larger than

516   expected due to not accounting for all of the horizontal temperature structure, which affects

517   forward radiance calculations through the Planck blackbody function, the retrievals of T(p), and

518   the registration of species radiance profiles with pressure. It may be that the V6 species

519   distributions within the SH have better accuracy from along its ascending (A) orbital segments,

520   since the tangent view paths for its profiles are more nearly in a zonal direction and do not have

521   significant T(p) gradients. Finally, we found no clear evidence of temperature bias in V6 NO_2.

522

523   Remsberg et al. (2013) reported that an assimilation of SBUV ozone along with the V6 A and D

524   Level 2 ozone profiles provides ozone distributions that agree well with balloon-sonde ozone in

525   the lower stratosphere. Yet, we do not recommend assimilation studies based on only the V6

526   ozone profiles because of their small, but persistent A-D differences, particularly at the edge of

527   and within the winter polar vortex. V6 H_2O profiles present similar assimilation problems.

528   Instead, we recommend that researchers make use of the average (A+D) V6 Level 3 product

529   and/or the SPARC-DI monthly, zonal average distributions for their science studies of

530   stratospheric ozone and H_2O, at least where NLTE effects are not an issue. As an example,

531   Tegtmeier et al. (2013) compared the combined V6 monthly stratospheric ozone distributions

532   with ones from other satellite-based limb sensors, and they found good agreement. Thereafter,

533   Shepherd et al. (2014) integrated the SPARC-DI V6 monthly zonal mean ozone above the

534   tropopause and subtracted it from observed total ozone as part of their assessment of long-term

535   trends of tropospheric ozone from models for 1978 and onward.

536

537   Remsberg et al. (2007, their Fig. 8b) found that zonal average V6 ozone in the middle

538   stratosphere is higher than SBUV ozone by 4%, which is well within the combined systematic

539   errors of both experimental datasets. Correlative ozone measurements for the middle to upper

540   stratosphere are too few and too inaccurate in 1978/1979 to determine whether the V6 A or D

541 ozone is more accurate. Thus, we considered V6 monthly profile data versus a monthly daytime

542 ozone climatology of the late 1970s obtained with the rocket-borne, uv-absorption (ROCOZ)

543 technique at Wallops Island, VA. We found agreement within their respective errors, except for

544 the uppermost stratosphere and the lower mesosphere. We also calculated time series of V6

545 Level 3 ozone and H_2O at 850 K and looked for consistency between their fields and those of

546 PV. In general, we found good agreement with similar studies of BR (1986) based on V5 data.

547 However, the time series from V6 shows better continuity during dynamically active periods.

548

549 The LIMS experience has been of benefit for the design of follow-on broadband, limb infrared

550 measurements. One satellite experiment, the Sounding of the Atmosphere using Broadband

551 Emission Radiometry (SABER), has been obtaining measurements of temperature, ozone, and

552 H_2O from 2002-2020 (e.g., Remsberg et al., 2008; Rong et al., 2009). Improvements from

553 SABER compared to LIMS are: (1) reductions in electronics and detector noise for its narrow-

554 band and wide-band CO_2 channels by factors of 5 and 16, respectively, and for its ozone channel

555 by a factor of 20; (2) common, 2-km IFOVs for its CO_2 (for temperature) and species channels to

556 account for diurnal temperature signals in the retrievals of ozone and H_2O; (3) an ozone filter

557 bandpass of about 1000 to 1150 cm^{-1} to avoid the NLTE emissions from the CO_2 laser band at

558 960 cm^{-1}; and (4) NLTE algorithms for retrievals of T(p), ozone, and H_2O in the mesosphere.

559 SABER instrument operation is stable and its orbital attitude information is accurate (Mlynczak

560 et al., 2020). SABER tangent view paths are 90° away from the spacecraft velocity vector or in

561 nearly a zonal direction for the low and middle latitudes, where zonal temperature gradients are

562 weak. There is little need to correct for T(p) gradients in the SABER algorithms, except when

563 viewing the high latitudes. Accordingly, diurnal temperature and ozone variations from SABER

564 compare reasonably with those from microwave measurements and with model estimates (e.g.,

565 Huang et al., 2010a and 2010b; Frith et al., 2020).

566

567 **Data Availability**

568 The LIMS V6 data archive is at the NASA EARTHDATA site of EOSDIS and its website:

569 https://search.earthdata.nasa.gov/search?q=LIMS). The ROCOZ ozone climatology at Wallops

570 Island is available from co-author, Arlin Krueger, upon request. The SPARC-Data Initiative site

571   is located at https://www.sparc-climate.org/data-centre/data-access/sparc-data-initiative/. We

572   acknowledge the individual instrument teams and respective space agencies for making their

573   measurements available, and the Data Initiative of WCRP's (World Climate Research

574   Programme) SPARC (Stratospheric Processes and their Role in Climate) project for organizing

575   and coordinating the compilation of the chemical trace gas datasets used in this work.

576

577   *Author Contributions.* ER prepared most of the figures and wrote the manuscript with

578   contributions from all co-authors. MN produced plots of the ascending minus descending

579   radiances. VLH prepared the time series plots of PV, ozone, and H_2O. AK provided his early

580   rocketsonde data on ozone and temperature and their estimated errors.

581

582   *Acknowledgements*. We are grateful to Krzysztof Wargan, who communicated to author ER in

583   2017 that he had concerns about the assimilation of alternating V6 A and D polar ozone profiles

584   during a re-analysis run of the MERRA model. We especially thank John Burton, L. L. Gordley,

585   B. T. Marshall, and R. E. Thompson for producing the V6 Level 2 dataset. Gretchen

586   Lingenfelser generated the V6 Level 3 zonal Fourier coefficient data. We thank John Gille and

587   Ernest Hilsenrath, who read and commented on a draft version of the manuscript. VLH

588   acknowledges support from NSF CEDAR grant 1343031, NASA LWS grant NNX14AH54G,

589   NASA HGI grant NNX17AB80G, and from NASA HSR grant 80NSSC18K1046. ER and MN

590   carried out their work while serving as a Distinguished Research Associates of the Science

591   Directorate at NASA Langley.

592   **References**

593   Barnett, J., and Corney, M.: Middle atmosphere reference model derived from satellite data, in

594   Handbook for Middle Atmosphere Program, Labitzke, K, Barnett, J. J., and Edwards, B., (Eds.),

595   vol. 16, 47-137, NASA Contractor Report 176321, Document ID 19860003346,

596   https://ntrs.nasa.gov, (last access November 12, 2019), 1985.

597

598   Brasseur, G., and Solomon, S.: Aeronomy of the Middle Atmosphere: Chemistry and Physics of

599   the Stratosphere and Mesosphere. 3rd ed., 644 pp., Springer, Dordrecht, Netherlands, 2005.

600

601   Butchart, N.: Evidence for planetary wave breaking from satellite data: the relative roles of

602   diabatic effects and irreversible mixing, in *Transport Processes in the Middle Atmosphere*,

603   Visconti, G., and Garcia, R. (Eds.), D. Reidel Publishing Co., Dordrecht, Holland, pp. 121-136,

604   1987.

605

606   Butchart, N. and Remsberg, E. E.: The area of the stratospheric polar vortex as a diagnostic for

607   tracer transport on an isentropic surface, J. Atmos. Sci., 43, 1319-1339,

608   https://doi.org/10.1175/1520-0469(1986)043%3C1319:TAOTSP%3E2.0.CO;2, 1986.

609

610   Dunkerton, T. J. and DeLisi, D. P.: Evolution of potential vorticity in the winter stratosphere of

611   January-February 1979, J. Geophys. Res. 91, 1199-1208,

612   https://doi.org/10.1029/JD091iD01p01199, 1986.

613

614   Edwards, D. P., Kumer, J. B., Lopez-Puertas, M., Mlynczak, M. G., Gopalan, A., Gille, J. C., and

615   Roche, A.: Non-local thermodynamic equilibrium limb radiance near 10 μm as measured by

616   UARS CLAES, J. Geophys. Res., 101, D21, 26,577-26,588, https://doi.org/10.1029/96JD02133,

617   1996.

618

Finger, F. G., Gelman, M. E., Schmidlin, F. J., Leviton, R., and Kennedy, V. W.: Compatibility of meteorological rocketsonde data as indicated by international comparisons tests, J. Atmos. Sci., 32, 1705-1714, https://doi.org/10.1175/1520-0469(1975)032%3C1705:COMRDA%3E2.0.CO;2, 1975.

Frith, S. M., Bhartia, P. K., Oman, L. D., Kramarova, N. A., McPeters, R. D., and Labow, G. J.: Model-based climatology of diurnal variability in stratospheric ozone as a data analysis tool, Atmos. Meas. Tech., 13, 2733-2749, https://doi.org/10.5194/amt-13-2733-2020, 2020.

Gille, J. C. and Russell III, J. M.: The limb infrared monitor of the stratosphere: experiment description, performance, and results, J. Geophys. Res., 84, 5125-5140, https://doi.org/10.1029/JD089iD04p05125, 1984.

Gille, J. C., Russell III, J. M., Bailey, P. L., Gordley, L. L., Remsberg, E. E., Lienesch, J. H., Planet, W. G., House, F. B., Lyjak, L. V., and Beck, S. A.: Validation of temperature retrievals obtained by the limb infrared monitor of the stratosphere (LIMS) experiment on NIMBUS 7, J. Geophys. Res., 89, 5147-5160, https://doi.org/10.1029/JD089iD04p05147, 1984.

Gordley, L. L. and Russell, J. M.: Rapid inversion of limb radiance data using an emissivity growth approximation, Appl. Opt., 20, 807-813, https://doi.org/10.1364/AO.20.000807, 1981.

Haigh, J. D., and Pyle, J. A.: Ozone perturbation experiments in a two-dimensional circulation model, Q. J. Roy. Meteorol. Soc., 108, 551-574, https://doi.org/10.1002/qj.49710845705, 1982.

Hitchman, M. H., and Leovy, C. B.: Diurnal tide in the equatorial middle atmosphere as seen in LIMS temperatures, J. Atmos. Sci., 42, 557-561, https://doi.org/10.1175/1520-0469(1985)042%3C0557:DTITEM%3E2.0.CO;2, 1985.

646

Huang, F. T., McPeters, R. D., Bhartia, P. K., Mayr, H. G., Frith, S. M., Russell III, J. M., and

Mlynczak, M. G.: Temperature diurnal variations (migrating tides) in the stratosphere and lower

mesosphere based on measurements from SABER on TIMED, J. Geophys. Res., 115, D16121,

https://doi:10.1029/2009JD013698, 2010a.

651

Huang, F. T., Mayr, H. G., Russell III, J. M., and Mlynczak, M. G.: Ozone diurnal variations in

the stratosphere and mesosphere, based on measurements from SABER on TIMED, J. Geophys.

Res., 115, D24308, https://doi:10.1029/2010JD014484, 2010b.

655

Kiefer, M., Arnone, E., Dudhia, A., Carlotti, M., Castelli, E., von Clarmann, T., Dinelli, B. M.,

Kleinert, A., Linden, A., Milz, M., Papandrea, E., and Stiller, G.: Impact of temperature field

inhomogeneities on the retrieval of atmospheric species from MIPAS IR limb emission spectra,

Atmos. Meas. Tech., 3, 1487–1507, https://doi.org/10.5194/amt-3-1487-2010, 2010.

660

Krueger, A. J.: The mean ozone distribution from several series of rocket soundings to 52 km at

latitudes from 58°S to 64°N, PAGEOPH, 106, 1272-1280, https://doi.org/10.1007/BF00881079,

1973.

664

Krueger, A. J: Inference of photochemical trace gas variations from direct measurements of

ozone in the middle atmosphere, Doctoral Dissertation, Colorado State Univ., Fort Collins, CO,

1984, (available for download from ResearchGate:

https://www.researchgate.net/publication/253654486_Inference_of_photochemical_trace_gas_va

riations_from_direct_measurements_of_ozone_in_the_middle_atmosphere).

670

671 Krueger, A. J. and Minzner, R. A.: A mid-latitude ozone model for the 1976 U. S. standard

672 atmosphere, J. Geophys. Res., 81, 4477-4481, https://doi.org/10.1029/JC081i024p04477,

673 1976.

674

675 Leovy, C. B., Sun, C-R., Hitchman, M. H., Remsberg, E. E., Russell, III, J. M., Gordley, L. L.,

676 Gille, J. C., and Lyjak, L. V.: Transport of ozone in the middle stratosphere: evidence for

677 planetary wave breaking, J. Atmos. Sci., 42, 230-244, https://doi.org/10.1175/1520-

678 0469(1985)042%3C0230:TOOITM%3E2.0.CO;2, 1985.

679

680 London, J., Frederick, J. E., and Anderson, G. P.: Satellite observations of the global distribution

681 of stratospheric ozone, J. Geophys. Res., 82, 2543-2556,

682 https://doi.org/10.1029/JC082i018p02543, 1977.

683

684 Lopez-Puertas, M. and Taylor, F. W.: Non-LTE Radiative transfer in the Atmosphere, World

685 Scientific Publ. Co., River Edge, NJ, USA, 504 pp., 2001.

686

687 Manuilova, R. O., Gusev, O. A., Kutepov, A. A., von Clarmann, T., Oelhaf, H., Stiller, G. P,

688 Wegner, A., Lopez-Puertas, M., Martin-Torres, F. J., Zaragoza, G., and Flaud, J.-M.: Modelling

689 of non-LTE limb spectra of i.r. ozone bands for the MIPAS space experiment, J. Quant.

690 Spectrosc. Rad. Transf., 59, 405-422, https://doi.org/10.1016/S0022-4073(97)00120-9, 1998.

691

692 Mertens, C. J., Mlynczak, M. G., Lopez-Puertas, M., and Remsberg, E. E.: Impact of non-LTE

693 processes on middle atmospheric water vapor retrievals from simulated measurements of 6.8 μm

694 Earth limb emission, Geophys. Res. Lett., 29 (9), 2-1 to 2-4,

695 https://doi.org/10.1029/2001GL014590, 2002.

696

697   Mlynczak, M. G., Daniels, T., Hunt, L. A., Yue, J., Marshall, B. T., Russell, J. M., III,

698   Remsberg, E. E., Tansock, J., Esplin, R., Jensen, M., Shumway, A., Gordley, L., and Yee, J.-H.:

699   Radiometric stability of the SABER instrument. Earth and Space Science, *7*, e2019EA001011,

700   https://doi.org/10.1029/2019EA001011, 2020.

701

702   Mlynczak, M. G. and Drayson, R.: Calculation of infrared limb emission by ozone in the

703   terrestrial middle atmosphere 2. Emission calculations, J. Geophys. Res., 95, 16,513-16,521,

704   https://doi.org/10.1029/JD095iD10p16513, 1990.

705

706   Remsberg, E., and Lingenfelser, G.: LIMS Version 6 Level 3 dataset, NASA-TM-2010-216690,

707   available at http://www.sti.nasa.gov (last access: 17 September 2019), 13 pp., 2010.

708

709   Remsberg, E. E., Haggard, K. V., & Russell , J. M., III. (1990). Estimation of Synoptic Fields of

710   Middle Atmosphere Parameters from Nimbus-7 LIMS Profile Data, *Journal of Atmospheric and*

711   *Oceanic Technology*, *7*(5), 689-705. Retrieved Jan 28, 2021,

712   from https://journals.ametsoc.org/view/journals/atot/7/5/1520-

713   0426_1990_007_0689_eosfom_2_0_co_2.xml, 1990.

714

715   Remsberg, E. E., Russell, J. M., III, Gille, J. C., Bailey, P. L., Gordley, L. L., Planet, W. G., and

716   Harries, J. E.: The validation of Nimbus 7 LIMS measurements of ozone, J. Geophys. Res., 89,

717   5161-5178, https://doi.org/10.1029/JD089iD04p05161, 1984.

718

719   Remsberg, E. E., Gordley, L. L, Marshall, B. T., Thompson, R. E., Burton, J., Bhatt, P., Harvey,

720   V. L., Lingenfelser, G., Natarajan, M.: The Nimbus 7 LIMS version 6 radiance conditioning and

721   temperature retrieval methods and results, J. Quant. Spectros. Rad. Transf., 86, 395-424,

722   https://doi.org/10.1016/j.jqsrt.2003.12.007, 2004.

723

724 Remsberg, E., Lingenfelser, G., Natarajan, M., Gordley, L., Marshall, B. T., and Thompson, E.:

725 On the quality of the Nimbus 7 LIMS version 6 ozone for studies of the middle atmosphere, J.

726 Quant. Spectros. Rad. Transf., 105, 492-518, https://doi.org/10.1016/j.jqsrt.2006.12.005, 2007.

727

728 Remsberg, E. E., Marshall, B. T., Garcia-Comas, M., Krueger, D., Lingenfelser, G. S., Martin-

729 Torres, J., Mlynczak, M. G., Russell III, J. M., Smith, A. K., Zhao, Y., Brown, C., Gordley, L.

730 L., Lopez-Gonzalez, M. J., Lopez-Puertas, M., She, C. Y., Taylor, M. J., and Thompson, E.:

731 Assessment of the quality of the Version 1.07 temperature versus pressure profiles of the middle

732 atmosphere from TIMED/SABER, J. Geophys. Res., 113, D17101,

733 https://doi.org/10.1029/2008JD010013, 2008.

734

735 Remsberg, E. E., Natarajan, M., Lingenfelser, G. S., Thompson, R. E., Marshall, B. T., and

736 Gordley, L. L.: On the quality of the Nimbus 7 LIMS Version 6 water vapor profiles and

737 distributions, Atmos. Chem. Phys., 9, 9155-9167, www.atmos-chem-phys.net/9/9155/2009/,

738 2009.

739

740 Remsberg, E., Natarajan, M., Marshall, B. T., Gordley, L. L., Thompson, R. E., and

741 Lingenfelser, G. S.: Improvements in the profiles and distributions of nitric acid and

742 nitrogen dioxide with the LIMS version 6 dataset, Atmos. Chem. Phys., 10, 4741–4756,

743 www.atmos-chem-phys.net/10/4741/2010/, 2010.

744

745 Remsberg, E., Natarajan, M., Fairlie, T. D., Wargan, K., Pawson, S., Coy, L., Lingenfelser, G.,

746 and Kim, G.: On the inclusion of Limb Infrared Monitor of the Stratosphere version 6 ozone in a

747 data assimilation system, J. Geophys. Res., 118, 7982-8000, https://doi.org/10.1002/jgrd.50566,

748 2013.

749

750 Roewe, D. A., Gille, J. C., and Bailey, P. L.: Infrared limb scanning in the presence of horizontal

751 temperature gradients: an operational approach, Appl. Opt., 21, 3775-3783,

752 http://dx.doi.org/10.1364/AO.21.003775, 1982.

753

754 Rong, P. P., Russell III, J. M., Mlynczak, M. G., Remsberg, E. E., Marshall, B. T., Gordley, L.

755 L., and Lopez-Puertas, M.: Validation of Thermosphere Ionosphere Mesosphere Energetics and

756 Dynamics/Sounding of the Atmosphere using Broadband Emission Radiometry

757 (TIMED/SABER) v1.07 ozone at 9.6 μm in altitude range 15–70 km, J. Geophys. Res., 114,

758 D04306, https://doi.org/10.1029/2008JD010073, 2009.

759

760 Russell, J. M., III, Gille, J. C., Remsberg, E. E., Gordley, L. L., Bailey, P. L., Drayson, S. R.,

761 Fischer, H., Girard, A., Harries, J. E., and Evans, W. F. J.: Validation of nitrogen dioxide results

762 measured by the Limb Infrared Monitor of the Stratosphere (LIMS) experiment on Nimbus 7, J.

763 Geophys. Res., 89, 5099-5107, https://doi.org/10.1029/JD089iD04p05099, 1984.

764

765 Sakazaki, T., Fujiwara, M., Mitsuda, C., Imai, K., Manago, N., Naito, Y., Nakamura, T.,

766 Akiyoshi, H., Kinnison, D., Sano, T., Suzuki, M., and Shiotani, M.: Diurnal ozone variations in

767 the stratosphere revealed in observations from the Superconducting Submillimeter-Wave Limb-

768 Emission Sounder (SMILES) on board the International Space Station (ISS), J. Geophys. Res.,

769 118, 2991-3006, https://doi.org/10.1002/jgrd.50220, 2013.

770

771 Shepherd, T. G., Plummer, D. A., Scinocca, J. F., Hegglin, M. I., Fioletov, V. E., Reader, M. C.,

772 Remsberg, E., von Clarmann, T., and Wang, H. J.: Reconciliation of halogen-induced ozone loss

773 with the total-column record, Nature Geoscience, 7, 443-449, https://doi.org/10.1038/ngeo2155,

774 2014.

775

776 Solomon, S., Kiehl, J. T., Kerridge, B. J., Remsberg, E. E., and Russell III, J. M.: Evidence for

777 nonlocal thermodynamic equilibrium in the ν_3 mode of mesospheric ozone, J. Geophys. Res.,

778 91, 9865-9876, https://doi.org/10.1029/JD091iD09p09865, 1986.

780 SPARC: The SPARC Data Initiative: Assessment of stratospheric trace gas and aerosol

781 climatologies from satellite limb sounders, Hegglin, M. I. and Tegtmeier, S., (Eds.), SPARC

782 Report No. 8, WCRP-5/2017, http://www.sparc-climate.org/publications/sparc-reports/, 2017.

784 Sun, C.-R., and Leovy, C.: Ozone variability in the equatorial middle atmosphere, J. Geophys.

785 Res., 95, 13,829-13,849, https://doi.org/10.1029/JD095iD09p13829, 1990.

787 Tegtmeier, S., Hegglin, M. I., Anderson, J., Bourassa, A., Brohede, S., Degenstein, D.,

788 Froidevaux, L., Fuller, R., Funke, B., Gille, J., Jones, A., Kasai, Y., Krüger, K., Kyrölä, E.,

789 Lingenfelser, G., Lumpe, J., Nardi, B., Neu, J., Pendlebury, D., Remsberg, E., Rozanov, A.,

790 Smith, L., Toohey, M., Urban, J., von Clarmann, T., Walker, K. A. and Wang, R. H. H.: SPARC

791 Data Initiative: A comparison of ozone climatologies from international satellite limb sounders,

792 J. Geophys. Res., 118, 12,229-12,247, https://doi.org/10.1002/2013JD019877, 2013.

794 WOUDC, World Ozone and Ultraviolet Radiation Data Centre, https://woudc.org/home.php.

795

796

Table 1

Estimates of Species Errors Due to Temperature Biases

799

Pressure (hPa)	100	50	10	3	1	0.4	0.1
Temperature Bias (K)	1.1	1.3	1.0	1.6	2.4	2.5	2.3
Ozone (%)	20	20	11	10	12	16	16
Water vapor (%)	16	18	8	15	--	--	--
Nitric acid (%)	5	1	1	6	--	--	--
Nitrogen Dioxide (%)	--	22	8	6	10	--	--
T(p) Diff (V6-BC) (K)	--	1.4	1.7	-4.4	-1.6	3.1	--

800

801

802

803

804

805
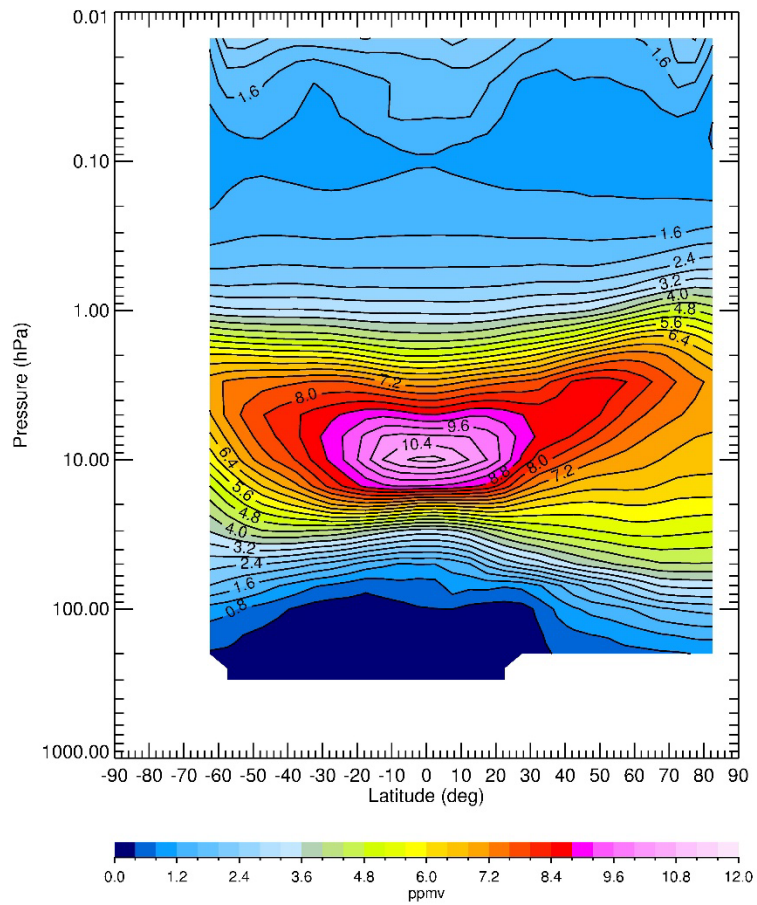
Figure 1—Zonal average ozone for March 1979 from the combination of the LIMS V6
ascending and descending orbital data. Contour interval (CI) is 0.4 ppmv.

808

809
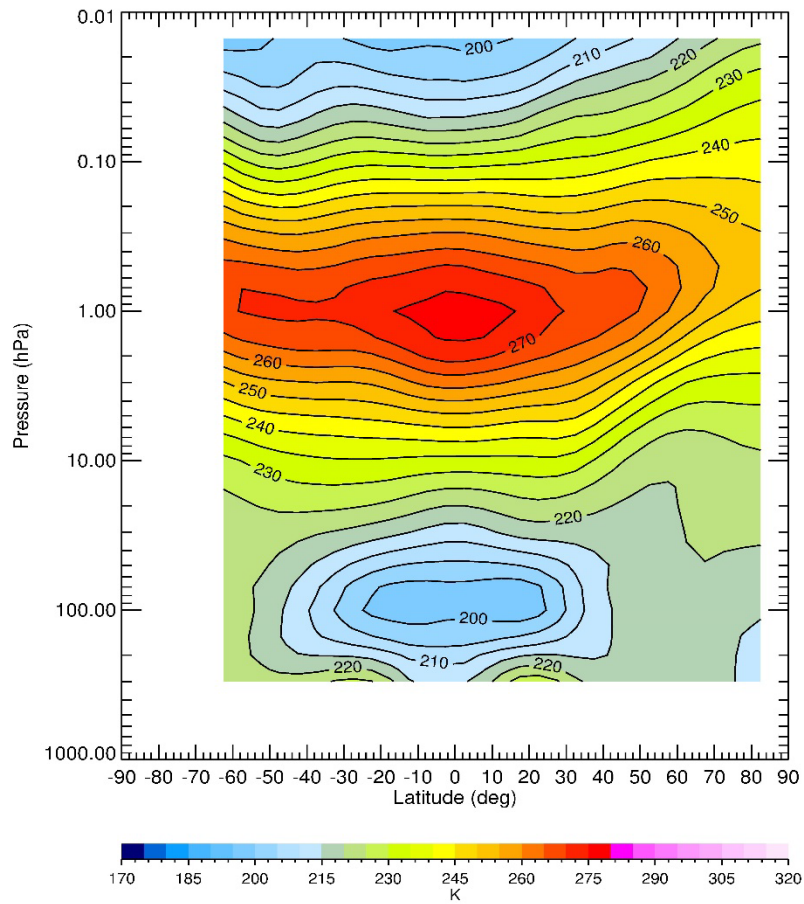
810

811   Figure 2—Zonal average temperature for March 1979. CI is 5 K.

812

813

814
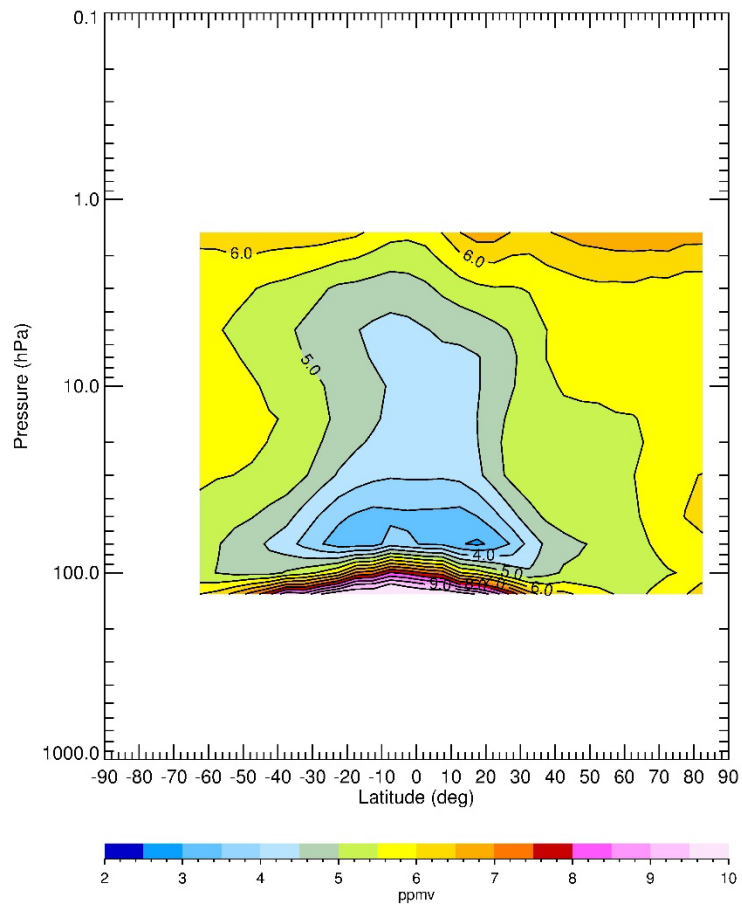
Figure 3—Zonal average water vapor for March 1979. CI is 0.5 ppmv.

816
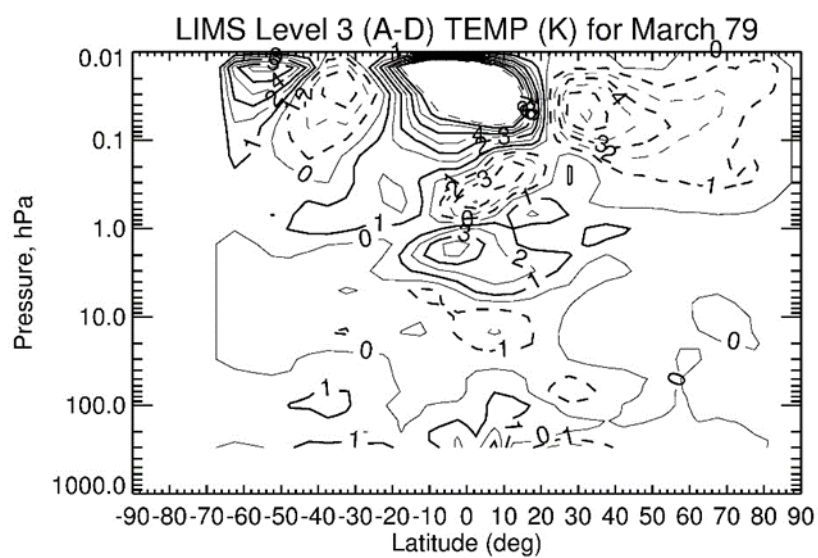
817

818   Figure 4—LIMS V6 Level 3 ascending minus descending (A-D) temperature differences (in K)

819   for March 1979. CI is 1 K and solid contours show positive differences.

820

821

822
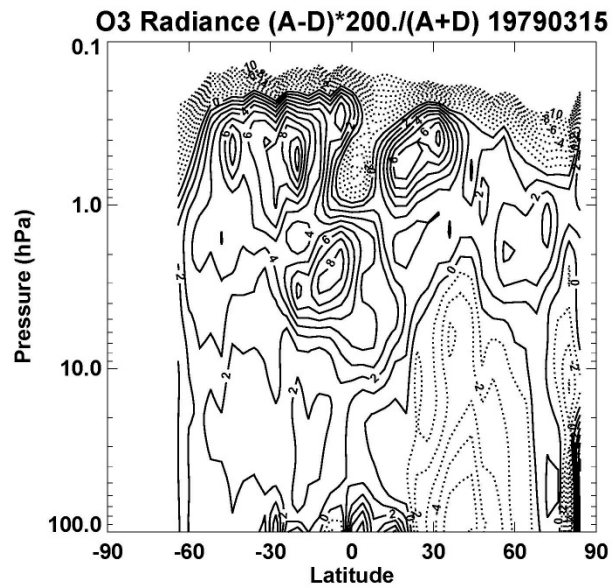
Figure 5—Ascending minus descending ozone radiance differences (in %) for March 15, 1979.
Contour interval is 1%.

825

826

827

828
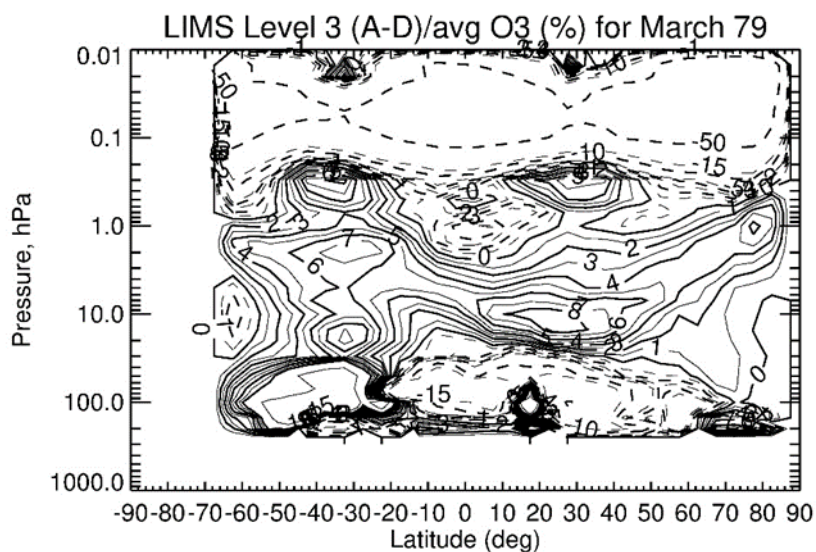
Figure 6—LIMS V6 Level 3 monthly zonal mean (A-D) ozone differences divided by average

ozone (and given in %) for March 1979. Solid contours are positive and CI is 1% from 0 to 10,

5% from 10 to 15, and then skipping to the 50% contour.

832

833
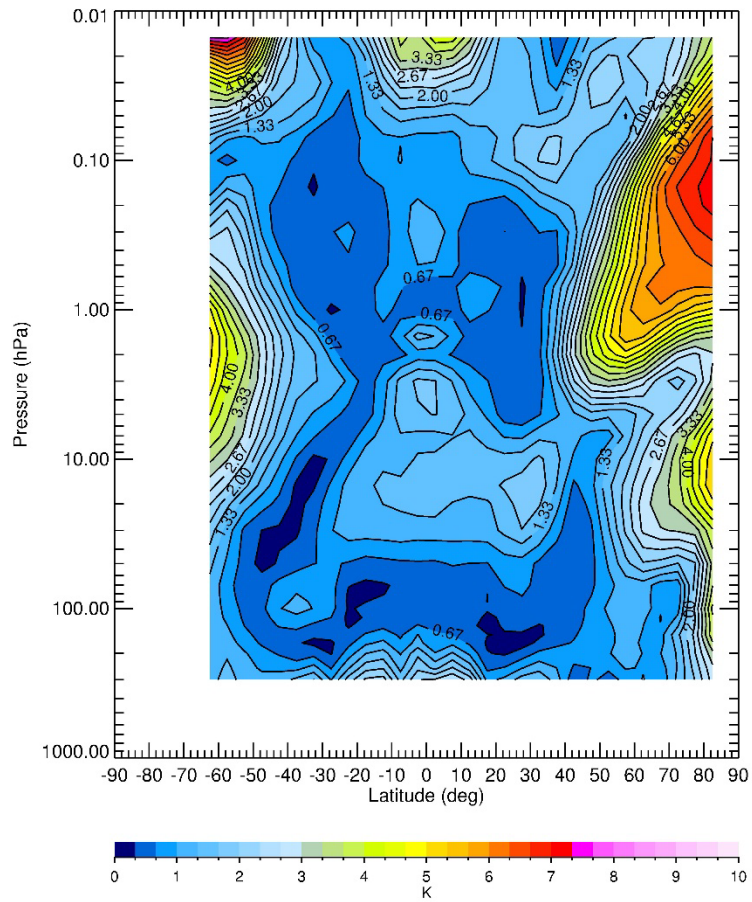
Figure 7—Average zonal (wave) standard deviation of temperature for March 1979. Contour

interval is 0.33 K.

836

837
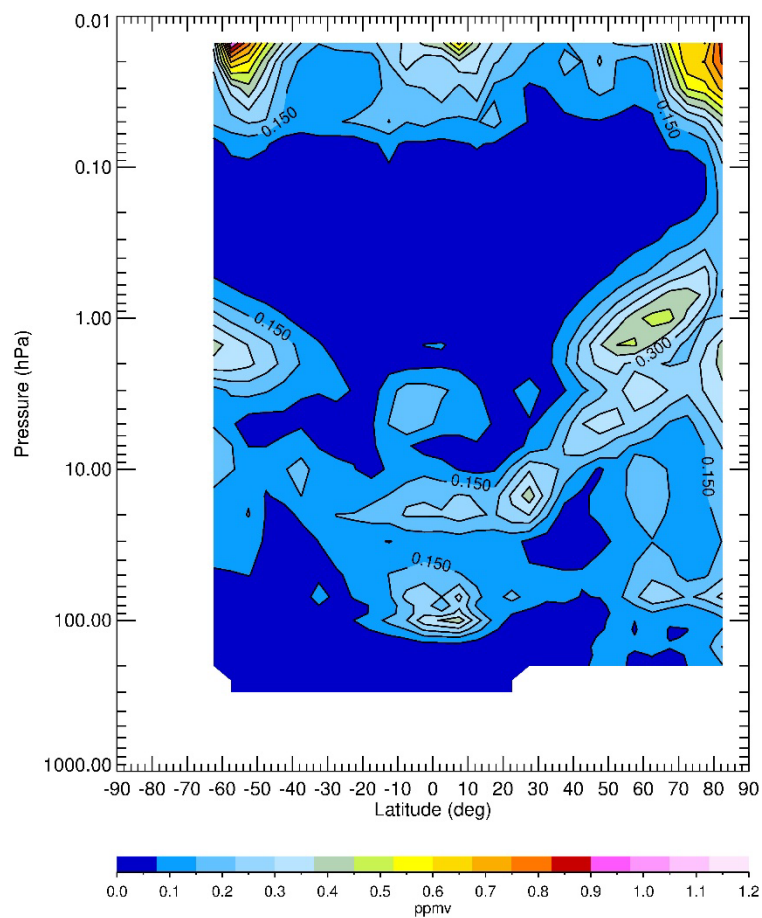
Figure 8—Average zonal (wave) standard deviation of ozone for March 1979. Contour interval

is 0.075 ppmv.

840

841

842
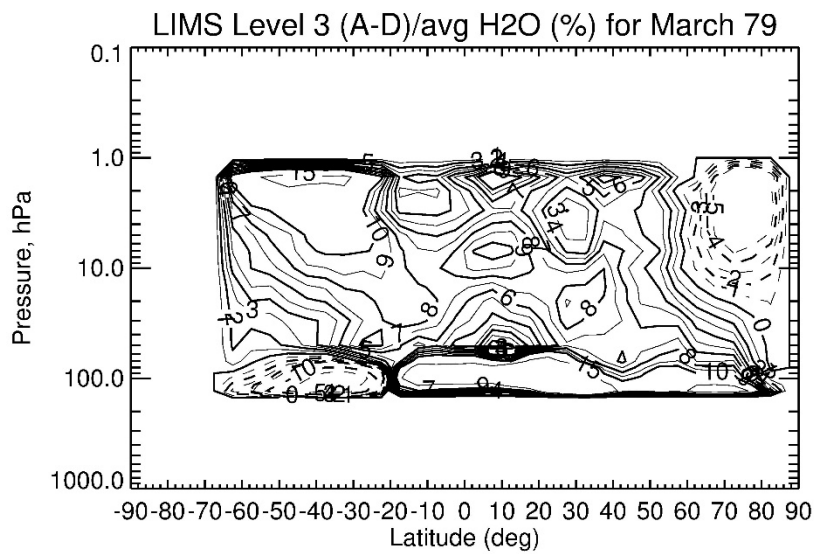
Figure 9—LIMS V6 Level 3 ascending minus descending (A-D) H_2O differences divided by

average H_2O (and given in %) for March 1979. CI is 1% from 0 to 10 and then 5% from 10 to

15; solid contours show positive differences.

846

847

848
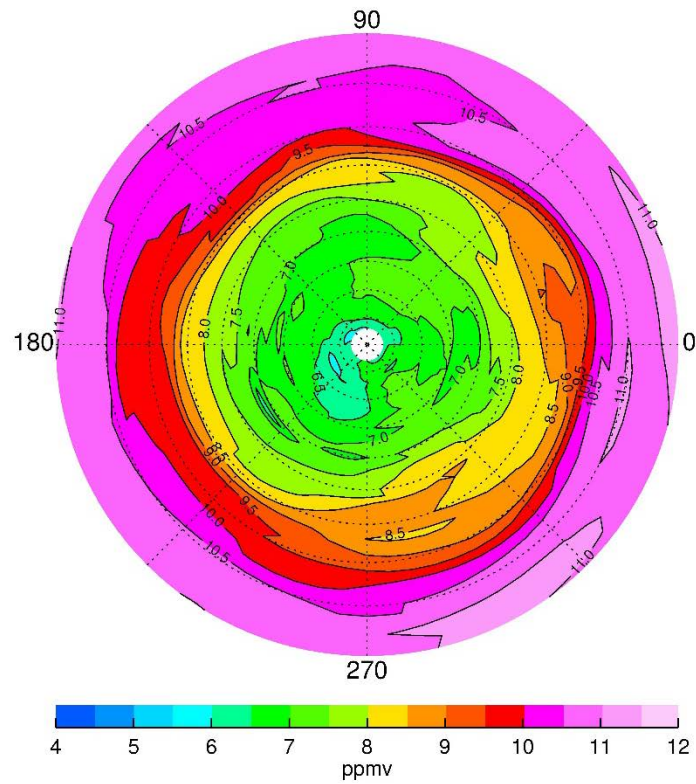
Figure 10—V6 ozone at 10 hPa for March 15, 1979, in the NH. Ozone contour interval is 0.5
ppmv, and latitude spacing (dotted circles) is 10°.

852

853

854
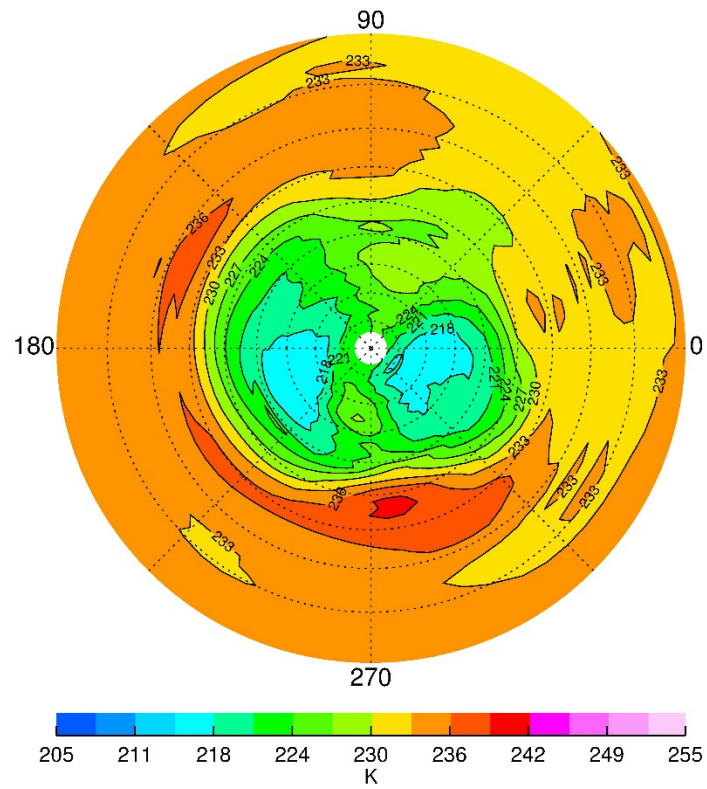
Figure 11—V6 temperature at 10 hPa for March 15, 1979, in the NH; contour interval is 3 K.

856

857

858

859
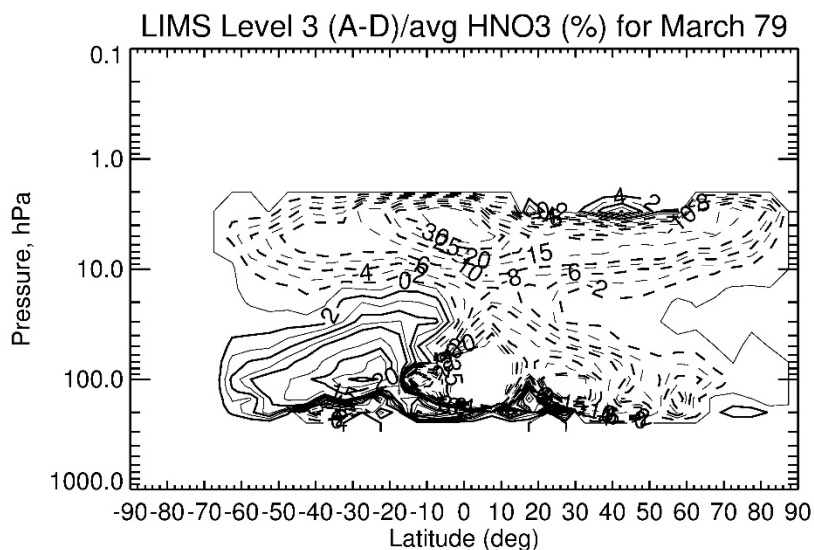
Figure 12—LIMS V6 Level 3 ascending minus descending (A-D) HNO₃ differences divided by
average HNO₃ (and given in %) for March 1979. CI is 2% from 0 to 10 and then 5% from 10 to
35; solid contours show positive differences.

863

864
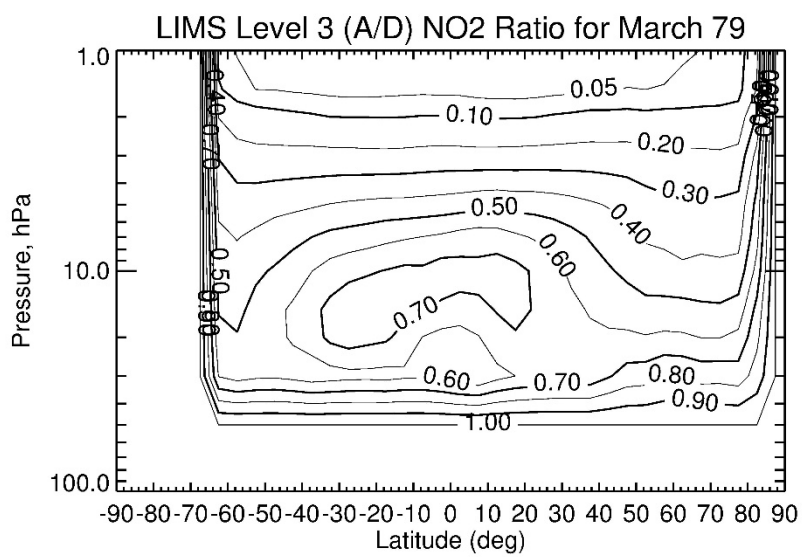
865

866   Figure 13—Distribution of the A to D ratios of V6 NO$_2$ for March 1979. CI is 0.05 (from 0.0 to
867   0.1) and then 0.1 (from 0.1 to 1.0).

868
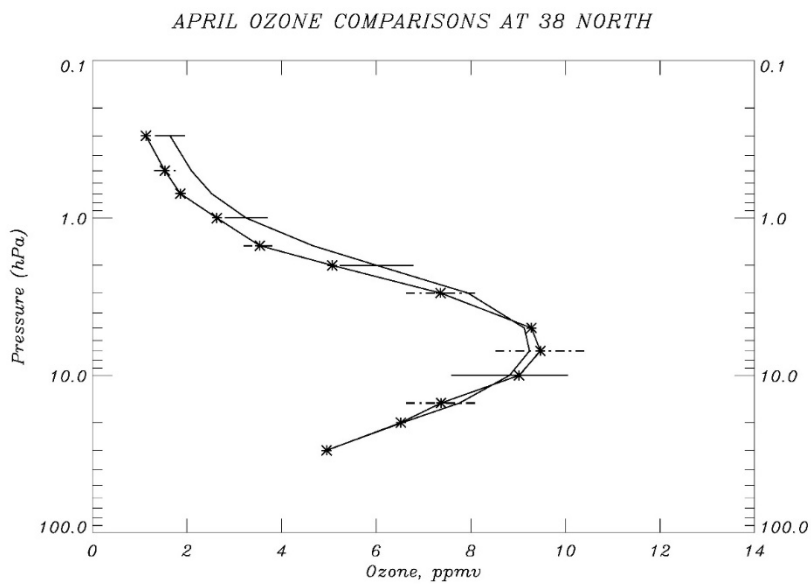
869

870

871   Figure 14—LIMS V6 monthly zonal mean daytime ozone (solid) for April 1979 at 38°N

872   compared with an average of three soundings (*) at Wallops Island, VA, 38°N, in April of 1976-

873   1978. Horizontal bars are error estimates for LIMS (solid) and for a ROCOZ sounding (dashed).

874

875

876
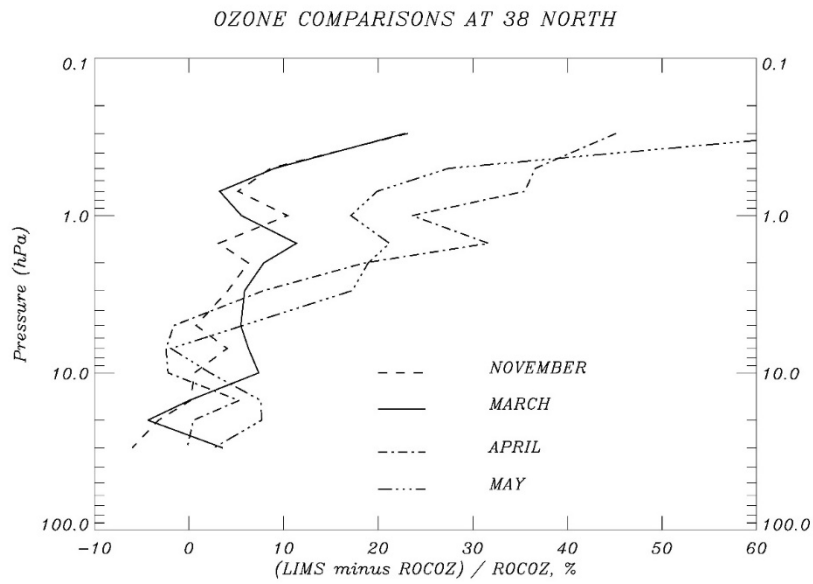
Figure 15—Monthly zonal mean V6 daytime ozone minus ROCOZ ozone (in %) for four months
at 38°N.

879

880

LIMS 850K PV (10⁻⁴m²s⁻¹Kkg⁻¹)

881
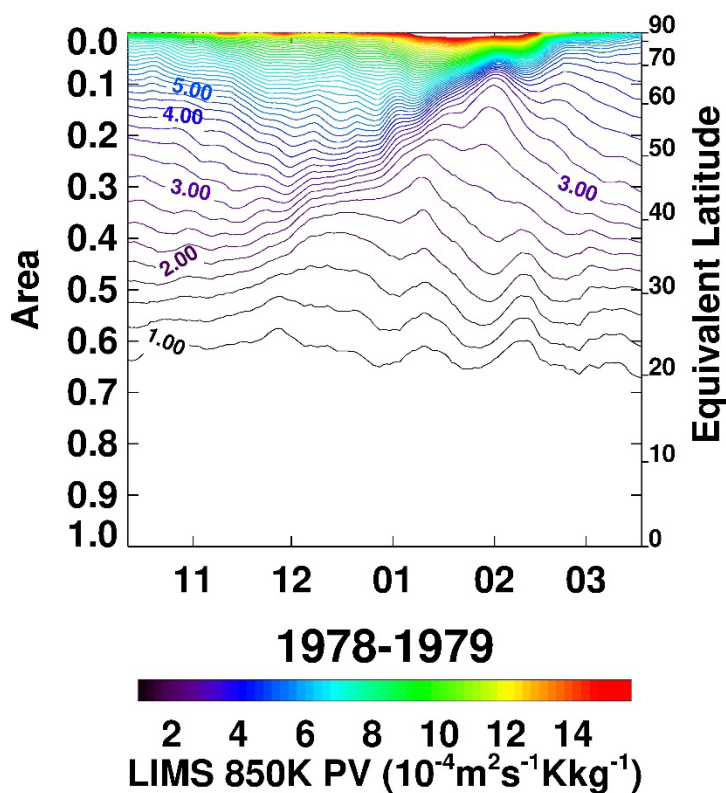
Figure 16—Area diagnostic plot of time series of NH potential vorticity (PV) contours on the

850 K potential temperature surface for comparison with Butchart and Remsberg (1986, their

Figure 4). PV comes from LIMS V6 Level 3 geopotential height and temperature data. Contour

interval (CI) is 0.25 PV units (units of PV are 10^{-4} m^2 s^{-1} K kg^{-1}). Tic marks on the abscissa

denote the 15th of each month.

887

888
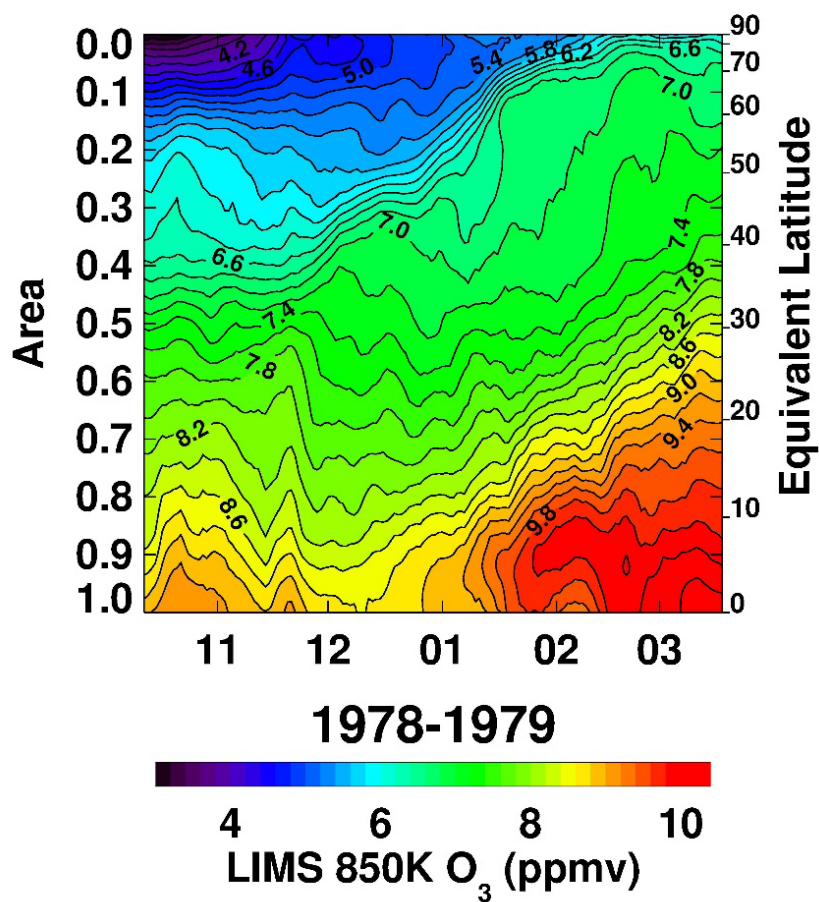
Figure 17—Area diagnostic plot of V6 Level 3 ozone for comparison with Figure 16. Ozone

contour interval is 0.2 ppmv. Tick marks on the abscissa indicate the 15th of each month.

892

893
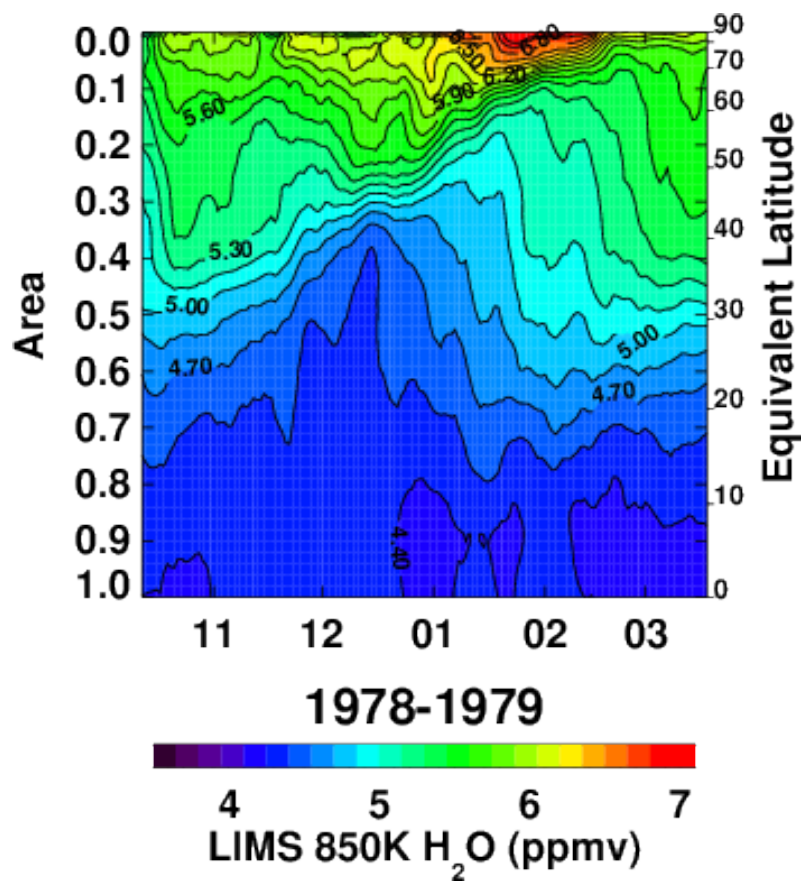
894

895   Figure 18—As in Fig. 17, but for V6 H_2O at 850 K; contour interval is 0.15 ppmv.

896